Proceedings of the IASTED International Conference
Modelling and Simulation
May 13-15, 1998, Pittsburgh, Pennsylvania - USA

INFLUENCE OF THE MATERIAL COMPOSITION AND DOPING PROFILES ON HBTS DEVICE PERFORMANCE

V. PALANKOVSKI, M. KNAIPP and S. SELBERHERR
Institute for Microelectronics, TU Vienna
Gusshausstrasse 27–29,A-1040 Vienna, AUSTRIA
Phone: +43/1/58801-3851, Fax: +43/1/5059224
E-mail: palankovski@iue.tuwien.ac.at

Abstract

Silicon Heterojunction Bipolar Transistors (HBTs) with SiGe narrow-gap base and GaAs HBTs with AlGaAs wide-gap emitter are simulated with a hydrodynamic (HD) transport model. The proper modeling of the physical parameters of the alloys allows a material composition profile optimization for different doping concentrations. With a TCAD framework the optimization can be automatically run in order to obtain the best electrical performance, e.g. maximum current gain and cut-off frequency.

1 INTRODUCTION

Recently the development of heterostructure devices has proceeded with very rapid steps. HBTs, Heterostructure Field-Effect Transistors (HFETs), optical detectors, and many other devices have derived great benefits from heterostructure technology. Significant improvements in the material properties and in the performance of the devices have been obtained. The applicability of the SiGe alloys in the silicon technology established an attractive class of HBTs based on Si, which show superior performance than the conventional Si BJTs, but inferior performance than the III-V compound semiconductor devices which are still receiving most attention for HBT research. Comparative analyses of different HBTs are of great importance for studying the device characteristics and are prerequisite for any device optimization.

2 PHYSICAL MODELS FOR COMPOUND MATERIALS

For accurate simulation of HBTs the respective temperature and mole fraction dependent models of the physical parameters of the alloys were implemented into MINIMOS-NT, our two-dimensional device simulator with approved capabilities of simulating devices with complex structure [1]. The correct modeling of the conduction and valence band-edge energies has basic importance for the simulation results. Band gap narrowing is one of the crucial heavy-doping effects to be considered for bipolar devices. Using the physically-based approach from [2], we implemented a model which considers the semiconductor material and the dopant species for arbitrary finite temperatures. The models for the effective density of states take into account material composition dependent electron and hole effective masses. The dielectric permittivity also varies with position. A new physically-based universal low field mobility model which distinguishes between majority and minority electron mobilities on one hand, and between different dopant species on the other hand, both as a function of temperature and dopant concentration was implemented. This unified treatment is especially useful for accurate device simulation.

In the following part of this section we present our physical models, which depend on the material composition, and therefore will be influenced by the optimization. In the simulation examples the models for the compound materials SiGe and AlGaAs were used.

2.1 PERMITTIVITY

In case of SiGe and AlGaAs a linear change in permittivity is assumed, thus for binary material $A_{1-x}B_x$ we use

$$\epsilon_r^{AB} = (1-x)\cdot\epsilon_r^{A} + x\cdot\epsilon_r^{B} \qquad (1)$$

In case of ternary material $A_{1-x}B_xC$ we have

$$\epsilon_r^{ABC} = (1-x)\cdot\epsilon_r^{AC} + x\cdot\epsilon_r^{BC} \qquad (2)$$

The parameters for the permittivity models of MINIMOS-NT are summarized in Table 1.

Material	ϵ_r^A	ϵ_r^B	ϵ_r^{AC}	ϵ_r^{BC}
$Si_{1-x}Ge_x$	11.9	16.0		
$Ga_{1-x}Al_xAs$			13.1	10.1

Table 1: Relative permittivity parameter values

2.2 DENSITY OF STATES

The transverse and the longitude electron masses (m_{nt} and m_{nl}), and the heavy and the light hole masses (m_{pl} and m_{ph}) are calculated in Eq. 3, where a linear variation with the material composition is assumed. With Eq. 4 and Eq. 5 we obtain the DOS masses for electrons and holes, respectively.

$$m_i = m1_i + m2_i \cdot x \tag{3}$$

$$\frac{m_n^*}{m_o} = \left(m_{nt}^2 \cdot m_{nl}\right)^{1/3} \tag{4}$$

$$\frac{m_p^*}{m_o} = \left(m_{pl}^{3/2} + m_{ph}^{3/2}\right)^{2/3} \tag{5}$$

The DOS masses are then used to obtain the conduction and valence band density of states Eq. 6 and Eq. 7.

$$N_C = 2 \cdot \left(\frac{2 \cdot \pi \cdot (m_n^*/m_o) \cdot k_B \cdot T}{h^2}\right)^{3/2} \cdot M_C \tag{6}$$

$$N_V = 2 \cdot \left(\frac{2 \cdot \pi \cdot (m_p^*/m_o) \cdot k_B \cdot T}{h^2}\right)^{3/2} \tag{7}$$

Here M_C is the number of energy valleys which for AlGaAs equals 6. The splitting of the energy valleys in case of SiGe is modeled by Eq. 8.

$$M_C^{SiGe} = 4 + 2 \cdot \exp\left(\frac{-0.6 \cdot x}{k_B \cdot T}\right) \tag{8}$$

The parameters for the effective density of states models are summarized in Table 2. For $x = 0$ we shall obtain the Si and GaAs values, respectively.

Material	m_i	m_{nt}	m_{nl}	m_{pl}	m_{ph}
$Si_{1-x}Ge_x$	$m1$	0.19	0.98	0.53	0.155
	$m2$	-0.108	0.66	-0.184	-0.113
$Al_xGa_{1-x}As$	$m1$	0.067	0.56	0.55	0.08
	$m2$	0.083	0.22	0.26	0.08

Table 2: Parameter values for modeling the effective density of states

2.3 BAND GAP ENERGIES

In case of SiGe the temperature dependence of the band gap in the pure materials is calculated with Eq. 9 and the results are put into Eq. 10 to account for arbitrary material composition.

$$E_g(T) = E_g(0) - \frac{\alpha \cdot T^2}{\beta + T} \tag{9}$$

$$E_g(x,T) = E_g^{Si}(T) \cdot (1-x) + E_g^{Ge}(T) \cdot x + C \cdot (1-x) \cdot x \tag{10}$$

For AlGaAs the material composition dependence of the band gap energy, α, and β in the compound material are calculated first, and then the temperature dependence is introduced with Eq. 14.

$$E_g(x,0) = E_g^{GaAs} \cdot (1-x) + E_g^{AlAs} \cdot x \tag{11}$$

$$\alpha(x) = \alpha^{GaAs} \cdot (1-x) + \alpha^{AlAs} \cdot x \tag{12}$$

$$\beta(x) = \beta^{GaAs} \cdot (1-x) + \beta^{AlAs} \cdot x \tag{13}$$

$$E_g(x,T) = E_g(x,0) - \frac{\alpha(x) \cdot T^2}{\beta(x) + T} \tag{14}$$

The conduction and valence band gap energies are calculated by

$$E_C(x,T) = E_g(0,T) + \frac{\partial E_C}{\partial E_g} \cdot [E_g(x,T) - E_g(0,T)] \tag{15}$$

$$E_V(x,T) = E_C(x,T) - E_g(x,T) \tag{16}$$

and the following parameters are used (see Table 3).

	α $[10^{-4}$eV/K]	β [K]	E_g [eV]	$\frac{\partial E_C}{\partial E_g}$	C [eV]
GaAs	5.58	220	1.521	0.6	
AlAs	8.78	332	2.891		
Si	4.73	636	1.1695	0.12	-0.4
Ge	4.774	235	0.74		

Table 3: Parameter values for modeling the band gap energies

Our band gap narrowing model considers the semiconductor material and the dopant species for arbitrary finite temperatures. Though band gap narrowing is very difficult to model rigorously, due to the multiple carrier interactions [3], one can approximate the energy shift by the classical self-energy of the electron in the field of an ionized impurity. Thus we obtain as a final expression for the band gap narrowing effect:

$$\Delta E_g = -\frac{e^2}{4 \cdot \pi \cdot \epsilon} \cdot [\beta \cdot N^* + \alpha_I \cdot N_I^* + \alpha_S \cdot N_S^*] \tag{17}$$

$$N^* = Z_I - \frac{N_I}{1 - \beta^2/\alpha_I^2} + \frac{Z_S \cdot \beta^2/\alpha_S^2}{1 - \beta^2/\alpha_{SC}^2} \tag{18}$$

$$N_I^* = N_I \cdot \left(\frac{1}{1 - \beta^2/\alpha_I^2} - 1\right) \tag{19}$$

$$N_S^* = N_S \cdot \left(1 - \frac{1}{1 - \beta^2/\alpha_S^2}\right) \tag{20}$$

The subscripts S and I refer to a semiconductor and impurity, respectively. Z and N are the atomic number and the number of electrons of a given material. α can be interpreted as size parameter of the electron

charge density, a_0 is the Bohr radius, and β denotes the inverse Thomas-Fermi length. They are expressed as

$$\alpha = \frac{Z^{1/3}}{c_k \cdot a_0 \cdot \epsilon_0 \cdot \epsilon_r} \cdot \frac{1 - 2 \cdot \left(\frac{Z}{N}\right)}{\frac{5}{3} - 4 \cdot \left(\frac{Z}{N}\right)^{1/3}} \tag{21}$$

$$c_k = \frac{\Gamma(4/3)}{2} \cdot \left(\frac{3 \cdot \pi}{4}\right)^{2/3} \cdot \left(\frac{3}{5}\right)^{7/3} \tag{22}$$

$$\beta^2 = \frac{n \cdot e^2}{\epsilon_0 \cdot \epsilon_r \cdot k_B \cdot T} \cdot \frac{F_{-1/2}(\eta)}{F_{1/2}(\eta)} \tag{23}$$

The Fermi integrals $F_{1/2}(x)$ are defined as in [4]. Using full Fermi-Dirac statistics in Eq. 23 the simulation results are valid for any doping concentration. Thus, our band gap narrowing model is the first theoretically derived model predicting different shifts for various dopant species.

2.4 MOBILITY MODELS

One of the basic assumptions in the models for ionized-impurity scattering is that the charge of an impurity center is treated as a point charge. In the approach from [2] it was shown that considering the spatial extent of the charge density one can explain various doping effects due to the chemical nature of the dopant at high doping concentrations. Based on Monte-Carlo (MC) simulation results for the low-field mobility in silicon, covering arbitrary finite concentrations, temperatures and dopants, analytical formulae for $\mu_n(N, T, Z)$, suitable for device simulation, were derived, e.g. in case of silicon we have

$$\mu_{\mathrm{n,maj}} = \frac{\mu_0 - g - h}{1 + \left(\frac{N_D}{C_1}\right)^{\alpha_1}} + \frac{g}{1 + \left(\frac{N_D}{C_2}\right)^{\alpha_2}} + h \tag{24}$$

$$\mu_{\mathrm{n,min}} = \frac{\mu_0 + m - k - h}{1 + \left(\frac{N_A}{C_1}\right)^{\alpha_1}} + \frac{k}{1 + \left(\frac{|N_A - C_a|}{C_2}\right)^{\alpha_2}} - \frac{m}{1 + \left(\frac{|N_A - C_b|}{C_3}\right)^{\alpha_3}} + h \tag{25}$$

where $\mu_0, \alpha_1, \alpha_2, \alpha_3, C_1, C_3, C_a, k$, and m are temperature dependent parameters, and g, h, C_2, and C_b are also dopant dependent [2].
Experimental data suggest a linear variation of the SiGe mobility with germanium fraction, and thus it can be modeled by

$$\mu_{SiGe}(x, \mu_{Si}) = \mu_{Si} \cdot (1.0 + K \cdot x) \tag{26}$$

where x denotes the germanium fraction [5]. The default value $K = 10.0$ is used.
In our HD 2-valley electron mobility model for III-V chemical group materials [6] the G- and L-valley low-field mobilities μ_n^{LI} are calculated. The temperature dependence is given by the change in the electron population P_L in the L-valley

$$P_L = 4 \cdot \left(\frac{m_L^*}{m_G^*}\right)^{3/2} \cdot \exp\left(-\frac{E_{C,L} - E_{C,G}}{k_B \cdot T}\right) \tag{27}$$

Here the relative masses m^* and conduction band edge energies E_C for G- and L-valley, respectively, are mole fraction dependent. Finally the HD mobility is found from

$$\mu_n^{HD}(x, T) = \frac{\mu_{n,G}^{LI} + \mu_{n,L}^{LI} \cdot P_L}{1 + P_L} \tag{28}$$

3 SIMULATION RESULTS

As a particular example, the electrical behavior of SiGe HBTs and AlGaAs HBTs was studied using a hydrodynamic transport model. Our investigations were performed in a comparative way for different concentrations. The simulation itself was started from the typical constant material composition $x = 0.2$ and base doping of $5e18\ cm^{-3}$ for both devices. The optimization was automatically run using our VISTA framework [7] with ten operating points distributed at equal distances of 11nm over the 100nm thick SiGe base of the Si HBT and over the 100nm thick AlGaAs emitter of the GaAs HBT, respectively. The constraints for the material composition values are set for the SiGe layer by the undesired effect of a strain relaxation. Therefore, the Ge fraction in the 100nm base region must not exceed 25%. For AlGaAs the band gap changes from direct to indirect gap with Al fraction higher than 40%. Thus, for the optimization we used 30% as maximum Al content. After comparison of the results for different base doping $1e19\ cm^{-3}$ was finally used. The goal of the optimization was to obtain the best figures-of-merit for a bipolar transistor, i.e. maximum current gain and cutoff frequency.
In Fig. 1 the Ge content in the base region of a Si HBT is shown before and after the optimization. Note, the absence of Ge on the base-to-emitter (BE) junction in the optimized profile. The benefit of graded material composition (starting from 0% at the BE junction) is well-known in practice. Now it was confirmed also by our simulation results. Fig. 2 shows the Al fraction before and after the optimization into the emitter of GaAs HBT. Note, the significant improvement of the current gain for both optimized devices and especially for the SiGe HBT (about two times for the whole range) in Fig. 3. The increase of the cutoff frequency obtained for the SiGe device can be seen in Fig. 4.

Acknowledgment

This work is supported by Siemens AG, Munich, Germany.

References

[1] T. Simlinger, H. Brech, T. Grave, and S. Selberherr. Simulation of Submicron Double-Heterojunction High Electron Mobility Transistors with MINIMOS-NT. *IEEE Trans.Electron Devices*, 44(5):700–707, 1997.

[2] G. Kaiblinger-Grujin, H. Kosina, and S. Selberherr. Influence of the Doping Element on the Electron Mobility in n-Silicon. *J.Appl.Phys.*, 15(3), 1998.

[3] E.F. Schubert. *Doping in III-V Semiconductors.* Cambridge University Press, 1993.

[4] D.K. Ferry. *Semiconductors.* Macmillan, 1991.

[5] D.M. Richey, J.D. Cressler, and A.J. Joseph. Scaling Issues and Ge Profile Optimization in Advanced UHV/CVD SiGe HBT's. *IEEE Trans.Electron Devices*, 44(3):431–440, 1997.

[6] R. Deutschmann. *Entwicklung eines physikalischen HFET-Modells: Parameterextraktion und Verifikation.* Dissertation, Technische Universität Wien, 1995.

[7] Ch. Pichler, R. Plasun, R. Strasser, and S. Selberherr. High-Level TCAD Task Representation and Automation. *IEEE Trans. Semiconductor Technology Modeling and Simulation*, May 1997. `http://www.ieee.org/journal/tcad/accepted/pichler-may97/`.

keywords: simulation, models, devices, optimization

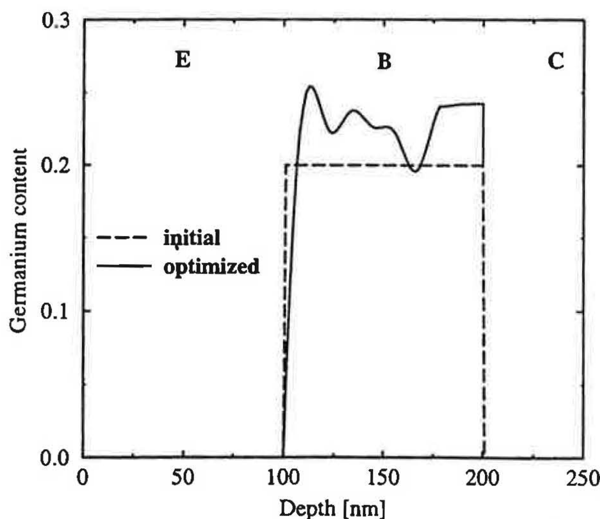

Figure 1: Material composition profile for SiGe HBT before and after optimization

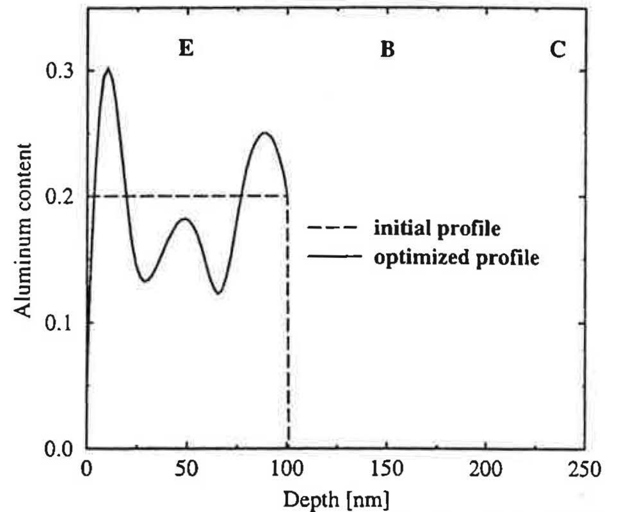

Figure 2: Material composition profile for GaAs HBT

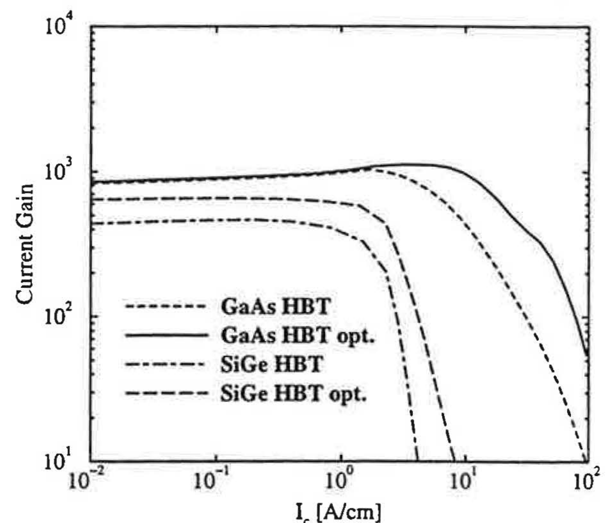

Figure 3: Current gain vs. collector current

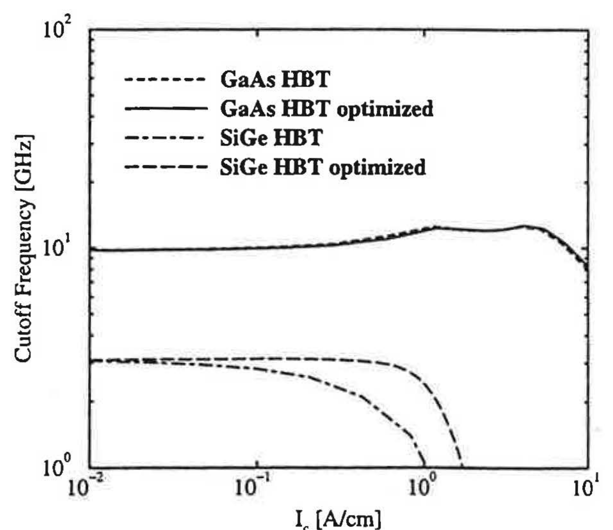

Figure 4: Cutoff frequency vs. collector current